OPTIMIZING THE PERFORMANCE OF MICROCOMPOSITES $Li_4Ti_5O_{12}$/Sn WITH Sn AND $Li_4Ti_5O_{12}$/Sn@C ANODE AND ACTIVATED CARBON CONTENT VARIABLES FOR LITHIUM-ION BATTERIES

Bambang Priyono[1*], Anne Zulfia Syahrial[1], Mohammad Ridho Nugraha[1], Dian Sepala[1], Faizah[1], Achmad Subhan[2]

[1]*Department of Metallurgy and Materials Engineering, Faculty of Engineering, Universitas Indonesia, Kampus UI Depok, Depok 16424, Indonesia*
[2]*Research Center of Physics, LIPI, PUSPIPTEK, Serpong, Tangerang Selatan, Banten 15314, Indonesia*

ABSTRACT

Lithium titanate ($Li_4Ti_5O_{12}$ or LTO) is a very promising anode material to replace graphite in li-ion batteries due to its safety and fast-charging ability. However, due to the low theoretical capacity of LTO, a strategy must be developed to overcome this problem. Synthesizing LTO by the combined sol-gel and solid-state method, and the addition of tin powder together with activated carbon, is expected to increase the specific capacity of the anode material. The tin powder compositions in this research were 5wt%, 7.5wt% and 12.5wt%. Further, to investigate the influence of activated carbon, 5wt%, 15wt%, and 25wt% activated carbon were added, while the composition of Sn was kept at 7.5wt%. XRD, SEM and BET surface area measurements was performed to characterize the morphology and structure of the samples. The performance of the battery was analyzed using EIS, CV and CD. The results show that TiO_2 rutile was present in the LTO samples, with peak rutile decreasing significantly with the addition of carbon. More disperse particle morphology was obtained by the addition of activated carbon. The LTO/Sn anode material exhibits excellent reversible capacities of 191.1 mAh/g at 12.5wt% tin. Additionally, the LTO/Sn@C has the highest specific-capacity at 270.2 mAh/g, with a composition of 5wt% carbon and 7.5wt% Sn. The results show that LTO/Sn@C is a potential anode material for the future.

Keywords: Activated carbon; Anode; $Li_4Ti_5O_{12}$/Sn; Sol-gel; Tin powder

1. INTRODUCTION

Lithium-ion batteries (LIBs) have diverse applications, ranging from powering electronic devices such as electric vehicles (EVs), to storing renewable energy (such as solar and wind energy) (Yi et al., 2014). State-of-the-art LIBs have used graphite-based material as part of the anode component due to its desirable charge potential profile, with the discharge capacity reaching 372 mAhg^{-1}, and lithium-insertion potential 0V (Li/Li$^+$) (Bayati et al., 2008). However, one of the limiting factors of graphite is its low lithiation potential, poor rate-capability and solvent co-intercalation, thus limiting its potential for EV development. The process of replacing graphite with $Li_4Ti_5O_{12}$ (LTO) has been developed to achieve optimal results. Spinel LTO is a good candidate because of its high lithium insertion voltage (1.5 VS (Li/Li$^+$)V), excellent safety profile, cycling performance due to its zero strain insertion

material (Priyono et al., 2015), and its applicability is high power conditions (Li et al., 2013). However, the specific capacity (175 mAh/g), electrical conductivity (10^{-13} S cm^{-1}) and lithium diffusion coefficient (10^{-9} to 10^{-13} cm^2 s^{-1}) of LTO is low (Ariyoshi et al., 2005). One of the ways to improve the performance rate is by reducing the particle size (Syahrial et al., 2018b), coating the surface with a more conductive material, such as carbon or silver (Kim et al., 2009) or by doping (Sofyan et al., 2016). In addition, tin oxide (Sn or SnO$_2$) can be used as the anode (Aurbach et al., 2002), whose theoretical capacity can reach up to 1491 mAhg^{-1}. However, the expansion of volume associated with the Sn charge-discharge process reaction of the newly formed metallic Sn with lithium, which leads to the formation of Li–Sn alloys with the composition of Li$_{4.4}$Sn, can reach 300% (Kim et al., 2009).

This volume expansion can lead to the collapse of the electrodes, ultimately decreasing capacity after several cycles (Crosnier et al., 2001). Several innovations have been studied by combining the nanoparticles of the Sn matrix to obtain the LTO-Sn composite (Egashira et al., 2002). In addition, increasing the surface area of the LTO-Sn composite could also be an alternative approach to improving battery performance. In this case, activated carbon is often used to increase the surface area due to its porous structure and ability to provide better support for the anode, since carbon matrices accommodate the change in volume of Sn during the charge–discharge process (Liang et al., 2011).

This paper focuses on optimizing the performance of anode batteries with LTO/Sn and LTO/Sn@C composites. The addition of Sn to LTO is aimed to increase specific capacity and reduce impedance. The LTO in this study was prepared by the sol-gel process and mixing of the Sn element using a ball-mill. Further, the addition of activated carbon is expected to produce LTO/Sn@C with evenly dispersed particles, in an effort to obtain good electrochemical performance. The effect of the tin powder and activated carbon on the LTO anode will be investigated.

2. METHODS

2.1. Material Preparation and Characterization

LTO powder was synthesized through the combined sol-gel and solid-state reaction route (Abdurrahman et al., 2017). Two micro-composites of anode materials were prepared for the study. The first anode material was 5wt%, 7.5wt%, and 12.5wt% LTO pure + tin powder using xerogel TiO$_2$ and LiOH precursors. The sol-gel process to prepare xerogel TiO$_2$ was conducted by making the primary solution with a combination of titanium tetra-n-butoxide (Kanto Chemical, Co. Inc.) and ethanol (Merck) and mixing it with the secondary solution, which contained ethanol and distilled water. The TiO$_2$ obtained was calcined at 300°C for 2 hours, then milled with a lithium source and sintered at 750°C for 3 hours under an argon flow to completely form a spinel structure LTO compound. To obtain LTO/Sn, the products were mixed with Sn powder at 5wt%, 7.5wt% and 12.5wt% by a milling process (Syahrial et al., 2018a). In this way, the first anode composite material was obtained. The second composite anode was LTO/Sn@C, comprising LTO, 5wt%, 15wt% and 25wt% activated carbon and 7.5wt% tin powder, with the starting materials being xerogel TiO$_2$ + activated carbon and LiOH. To obtain LTO/Sn@C, the preparation procedure was the same, apart from the addition of activated carbon during the sol-gel preparation of xerogel TiO$_2$ to make the uniform distribution of the activated carbon within TiO$_2$ framework. Sample specimens were initially characterized using X-ray diffraction (XRD) using Cu Kα radiation. The LTO powder was observed by scanning the electron microscope Hitachi SU-3500 with EDS to analyze the morphology and composition of the sample. Further characterization was performed using the Brunauer–Emmett–Teller (BET) method in order to analyze the surface area of the LTO with a Quantachrome Nova instrument.

2.2.   Electrochemical Measurement

For electrochemical characterization, the composite electrodes were fabricated by mixing the active materials, carbon black and polyvinylidene fluoride (PVDF) dissolved in dimethylacetamide (DMAC) solvent at a weight ratio of 80:10:10. The slurries were deposited on current collectors using copper foil by Doctor Blade at 6 cm/minute coating speed. The electrode was then dried under vacuum at 80°C for 2 h before electrochemical testing. Cell assembly was performed in an argon-filled glove box. Electrochemical performances were measured using a CR2032-type coin cell with lithium metal as the counter electrode. The electrolyte used was LiPF$_6$. Electrochemical impedance spectroscopy (EIS) was conducted, ranging from 100 kHz to 10 MHz using a HIOKI RM3544 instrument, while a cyclic voltammetry (CV) test was performed between 0.01 and 3.0 V with a scan-rate of 0.10 mVs^{-1}. The charge-discharge (CD) performance was conducted from low current (C/5) to high current (12C) discharge rate using a WonATech WBCS 2000 instrument.

The samples containing LTO and Sn were designated as LS with 3 compositions: LS5, LS7.5 and LS12.5, representing 5wt.%, 7.5wt.% and 12.5 wt.% of Sn. In addition, the samples containing LTO, Sn and activated carbon were designated as LSC with three compositions: LSC5, LSC15 and LSC25, representing 5wt.%, 15wt.% and 25 wt.% of C, with Sn kept constant at 7.5%. The LTO would be the remaining composition. Therefore, in total there were six samples.

3.   RESULTS AND DISCUSSION

3.1.   XRD Pattern of LTO Materials

X-ray diffraction studies were performed to find a relationship between the electrochemical properties and the structure of the LTO powder. XRD testing was used to detect the presence of the three phases, i.e., LTO, Sn and carbon. An expected phase in the XRD pattern was the spinel Li$_4$Ti$_5$O$_{12}$, with the analysis made by X-pert High Score Plus software. As shown in Figure 1, the 2θ peaks at 35.81°, 43.47°, 57.45°, 63.07° and 66.30° correspond to JCPDS no. 00-049-0207 spinel Li$_4$Ti$_5$O$_{12}$ (LTO). The peaks at 25.52°, 38.00° and 54.32° match 01-073-1764 (TiO$_2$ anatase), those at 27.75° and 54.32° correspond to 01-078-1510 (TiO$_2$ rutile), while the peaks at 30.07° 32.13° and 45.14° correspond to 03-065-0296 (Sn).
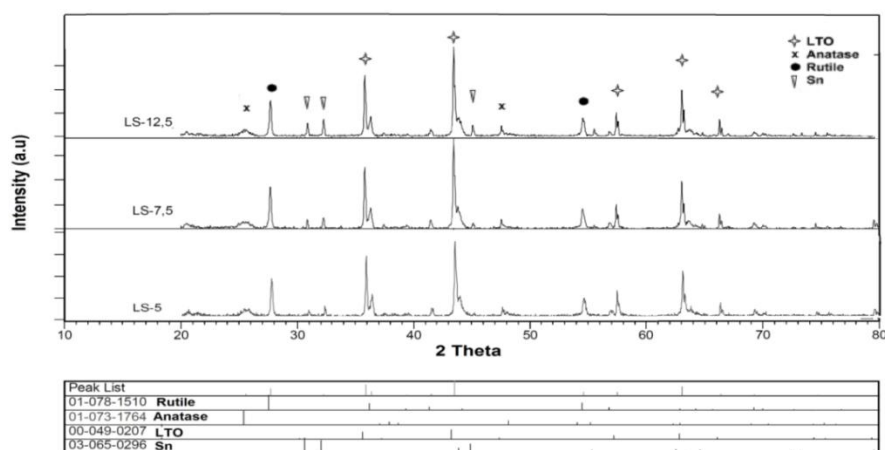

Figure 1 XRD patterns of LTO/Sn powder with tin content of 5 wt.%, 7.5 wt.% and 12.5 wt.%

From the results shown above, the spinel LTO phase was successfully identified in five angle position of 2θ. In Figure 1, it is shown that four compounds were formed, i.e. LTO, TiO$_2$ anatase, TiO$_2$ rutile and Sn, but that the LTO synthesized was not pure. The impurities present are TiO$_2$ anatase, as indicated by the peak at 25.4°, and TiO$_2$ rutile, since there are two rutile peaks at 27.6° and 63°. LTO peaks were obtained, of which the highest are at 35.8° and 43.5° and, at the same

time, there are Sn peaks at 30.07° and 32.20°. The LTO peak does not change or shift when Sn is added, thus indicating that they are coexisting. The presence of TiO_2 anatase and rutile in the XRD pattern shows the remaining TiO_2, which does not react with LiOH. The lack of reaction of TiO_2 with LiOH could be caused by the source of Li being exhausted, thus the TiO_2 anatase will turn into TiO_2 rutile. Anatase is a metastable phase of TiO_2, whereas rutile is a stable phase.

After Rietveld refinement using HighScore Plus software, the phase percentages are listed in Table 1.

Table 1 Phase percentages in LS5, LS 7.5, and LS12.5

No	Sample	% LTO	%Anatase	%Rutile	%Tin
1	LS-5	66.7	1.9	30.4	1.0
2	LS-7.5	67.8	2.5	28.1	1.6
3	LS-12.5	70.5	1.4	25.5	2.6

Further, in Figure 2 it is shown that the peak at 2θ at 32.22° corresponds to JCPDS 00-018-0311 (carbon). In the standard peak list of JCPDS 00-018-0311, there is a peak at 31.93°. Therefore, this peak probably convolutes with the Sn peak, as listed in JCPDS 03-065-0296 at 32.13°. That is why the peak intensity at 32.22° increases with the increased addition of carbon. This could be the best prediction of this finding.
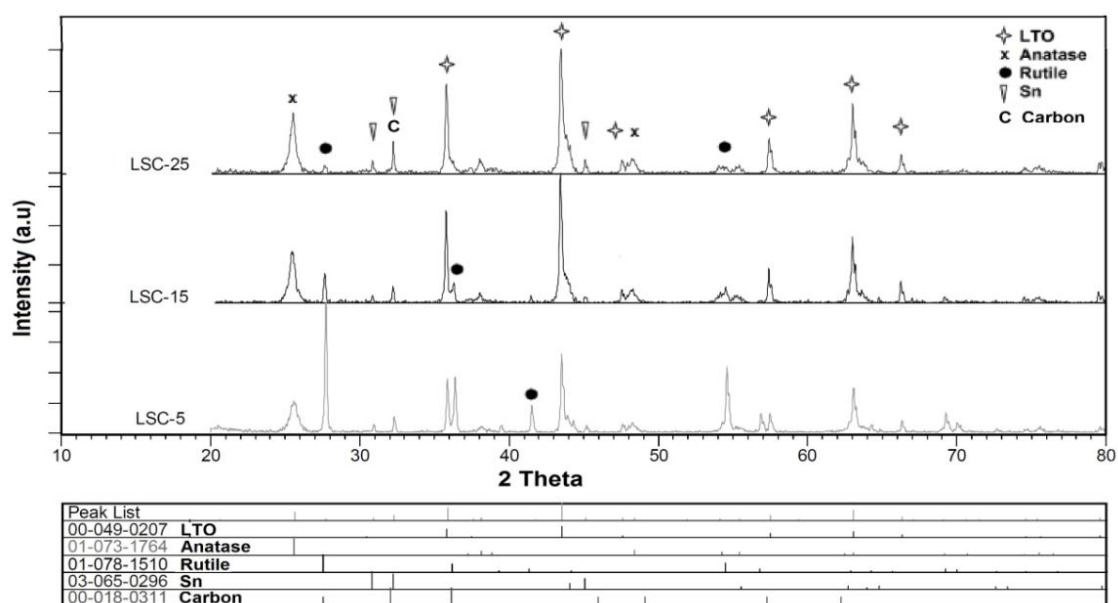

Figure 2 XRD patterns of LTO/Sn@C at 5 wt.%C, 15 wt.%C and 20wt.% C sample powder with tin content of 7.5 wt% Sn

After Rietveld refinement using HighScore Plus software, the phase percentages in the LSC samples are listed in Table 2.

Table 2 Phase percentages in LSC5, LSC 15, and LSC25

No	Sample	% LTO	%Anatase	%Rutile	%Tin	%C
1	LSC-5	0.8	36.9	59.7	1.0	1.5
2	LSC-15	59.6	26.2	8.3	1.0	4.9
3	LSC-25	63.7	24.9	1.7	1.2	8.5

In addition, as shown in Figure 2, in the samples with carbon added to the composition, the peak rutile is significantly reduced and the anatase peak is still present after sintering at 750°C. It is very interesting that the rutile phase is affected by the addition of carbon and suppresses its peak intensity. The presence of anatase and rutile was mainly due to the exhaustion of the LiOH source in the formation reaction of LTO, and unreacted TiO_2 could be present as anatase, rutile, or both. The presence of carbon has stabilized the anatase phase. This finding is in line with the work on the preparation of anatase coated with carbon by previous researchers to investigate photocatalytic activity, i.e.: in the carbon-coated TiO_2 sample, from the XRD data patterns of the anatase, TiO_2 is found, even after heating at 800°C, although a small amount of the rutile-type structure appears (Chen & Bae, 2006). This confirms that there is anatase phase stability with the addition of carbon. For comparison, in previous research on the preparation of LTO without carbon content, rutile has only been found as an impurity, and no anatase is present after sintering at 750°C (Priyono et al., 2015).

3.2. BET Surface Area

BET analysis shows that most of the LTO samples produced have been on the surface area have used active carbon that reaches 222.85 m^2/g. This value is higher in comparison to just within the surface area of the LTO was only 30.83 m^2/g. Addition of carbon in amount of 5wt.% to LS 7.5 makes the surface area still under the surface area of original LTO. The addition of 5% activated carbon is to LTO/Sn (7.5% Sn), not to the LTO alone. Thus, the particle of Sn may reduce the surface area compare to the original LTO. It makes the addition of 5% activated carbon does not sufficiently increase the surface area. By further increasing the active carbon to 15wt% and 25wt%, the surface area increased to 34.47 and 53.42 m^2/gr.

Table 3 Surface area of LTO samples with the addition of activated carbon

Sample	Surface area (m^2/g)
CA	222.85
LTO	30.83
LSC-5	23.64
LSC-15	34.47
LSC-25	53.42

3.3. SEM Images and EDS of the LTO Samples

The morphologies of the LTO spinel are shown in Figure 3. From these, it is apparent that the morphologies of all the samples are similar, and the SEM images of all the samples show how small and uniform the particle dimensions formed are.
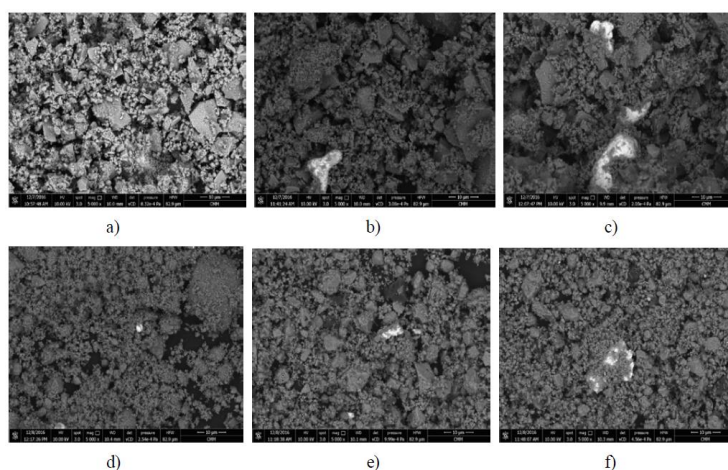

Figure 3 SEM images of LTO/Sn and LTO/Sn@C powder from samples: (a) LS-5; (b) LS-7.5; (c) LS-12.5; (d) LSC-5; (e) LSC-15; and (f) LSC-25, at 5000× magnification

In Figure 3, the SEM images were obtained using the backscattered electron (BSE) method. This method is intended to visually determine the elements contained in the sample, which is further confirmed using EDS testing. The heavy elements will be lighter in color than the lighter ones. Therefore, in these backscattered SEM images, three colors should be observed: grey is LTO, bright white is Sn, and dark grey or black is carbon. The LTO sample in Figure 3a is that with 5wt% addition; there is no noticeable color difference, indicating no visible Sn. This means the Sn is mixed evenly or homogeneously. The slightly brighter color in Figure 3a is because the brightness used to take the image was higher than that of the other samples. In Figures 3b−3f, the brightness and contrast of the Sn are arranged in such a way to show the different colors of Sn and other elements. The observation at 5000× magnification shows that with the addition of carbon, the grains become finer. Large agglomerates decrease slightly in the presence of carbon.
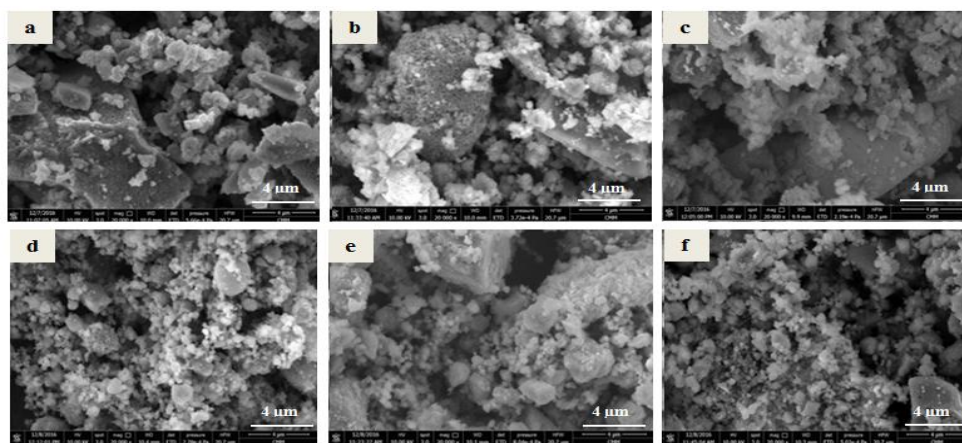

Figure 4 SEM images of LTO/Sn and LTO/Sn@C powder from samples (a) LS-5, (b) LS-7.5, (c) LS-12.5, (d) LSC-5, (e) LSC-15, and (f) LSC-25, at 20000× magnification

For a better view, the other sample images are presented at higher magnification, as seen in Figure 4, in order to show the morphologies of the LTO/Sn and LTO/Sn@C powders, which are prepared by the same method, by mixing the Sn element using a ball-mill. The SEM images above the surface show many large agglomerates and any difference in grain size is not significant after the addition of Sn in amounts of 5wt%, 7.5wt% and 12.5wt%. This is reasonable, since the process of grain growth and agglomeration occurs only in the sintering process in the formation of LTO, but does not occur during the mixing of LTO and Sn by high speed ball milling for 15 minutes. The addition of carbon in the LTO/Sn sample, as seen in Figures 4d, 4e and 4f, suppresses the agglomeration in LTO, as there are more tiny particles around the large particles. The tiny particles attached to the surface of the large agglomerates could also be fragments of large agglomerates as a result of the milling.

The imageJ particle size analysis was conducted using SEM images with 5000× magnification. First, the scale of the image was calibrated, the band-pass filter processed, and the image threshold adjusted. After the outline of each particle was set, the surface area of the particles could be obtained. Since the shape of the particles is irregular, the circularity is set as wide as possible using the default value. The surface area of each particle captured in the images was obtained and processed using a descriptive statistic method to obtain the average particle size, as shown in Table 4. All particle shapes are assumed to be square.

Table 4 Average particle size of the samples analyzed using imageJ

No	Sample	Average particle size (μm)
1	LS-5	1.267 ± 0.038
2	LS-7.5	1.159 ± 0.061
3	LS-12.5	0.522 ± 0.015
4	LSC-5	0.420 ± 0.024
5	LSC-15	0.158 ± 0.006
6	LSC-25	0.140 ± 0.002

The addition of Sn decreases the particle size of the sample. The same effect is also observed with addition of activated carbon. The reduction in particle size could be advantageous to anode performance (Syahrial et al., 2018b).

EDS testing was also conducted to confirm the presence of LTO, Sn and carbon particles; the results are presented in Figures 5, 6 and 7.
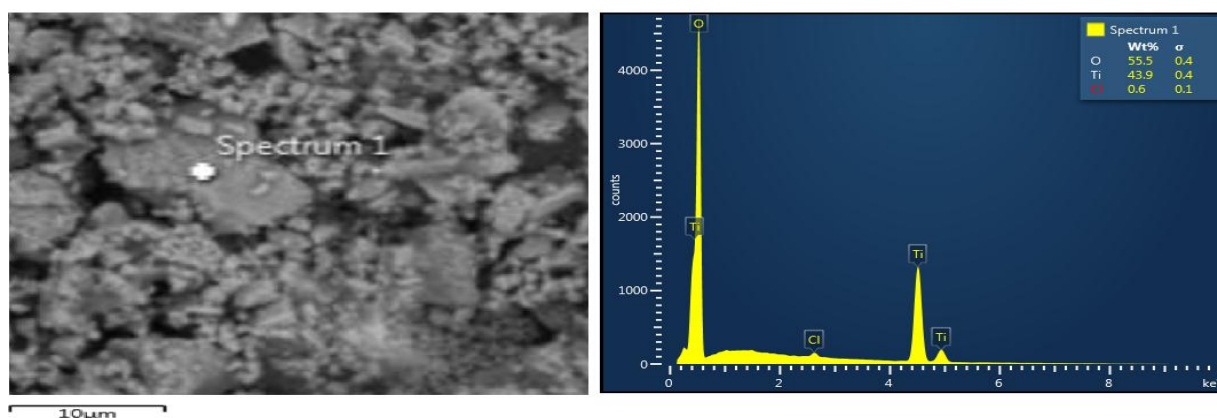

Figure 5 EDS test results of sample LS-5 to confirm the existence of LTO particles

As seen in Figure 5, spectrum 1 spotlighted at a certain particle and the EDS results show the Ti content as 43.9 wt.% and that of oxygen at 55.5wt%, confirming the presence of LTO particles. The lithium content cannot be detected by EDS due to its atomic weight.
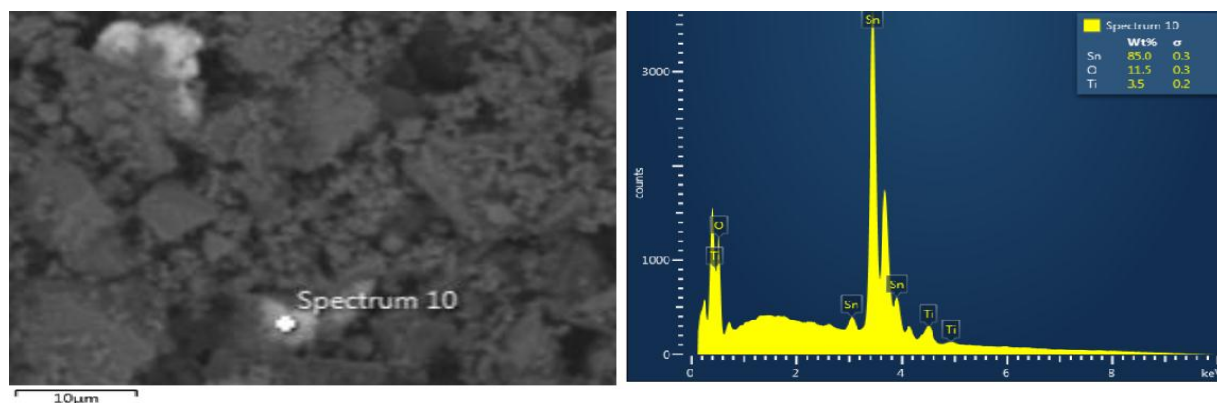

Figure 6 EDS test results of sample LSC-12.5 to confirm the existence of Sn particles

Figure 6 shows spectrum 10 spotlighted at a certain bright particle, and the EDS results show the Sn content to be 85.0 wt.% with oxygen at 11.5wt%, confirming the presence of Sn particles.
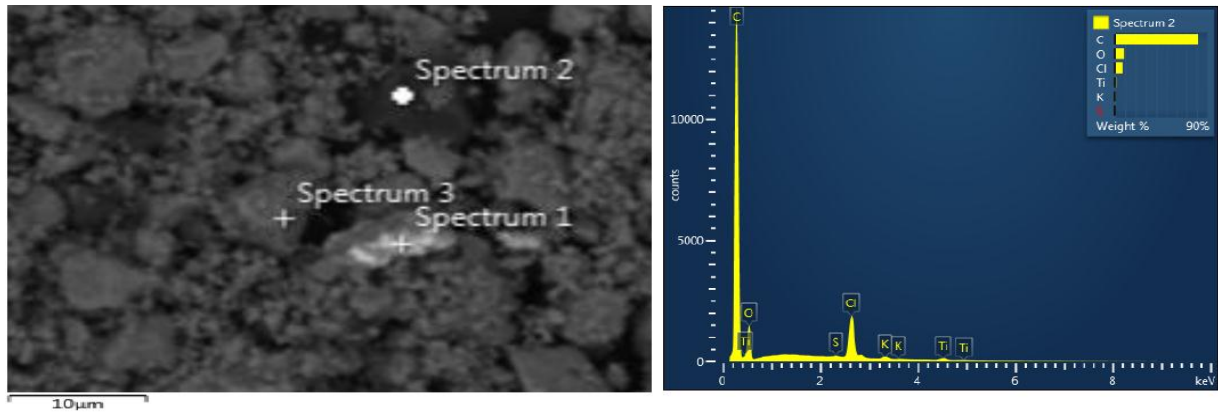
Figure 7   EDS test results of sample LSC-12.5 to confirm the existence of carbon particles

In Figure 7, spectrum 2 spotlighted at a certain dark particle. The EDS results show the carbon content to be 90.0 wt.%, with that of oxygen much lower, confirming the presence of carbon particles.

3.4.   EIS Characterization of the LTO Electrodes

Electrochemical impedance (EIS) analysis was conducted to investigate the Rs (solution impedance), the charge transfer impedance (Rct) and diffusion process or Warburg diffusion factor. The Nyquist semicircle of the sample cells studied is shown in Figure 8. In the LTO/Sn samples, Figure 8 shows that the composition with 12.5wt% Sn has the lowest resistivity values, while LTO/Sn-7.5 shows the highest. In the LTO/Sn@C samples, all the results show higher resistivity compared to LTO/Sn. Therefore, the addition of activated carbon increases resistivity. The highest resistance value is in the LSC-5 sample, while the lowest is in LSC-15.
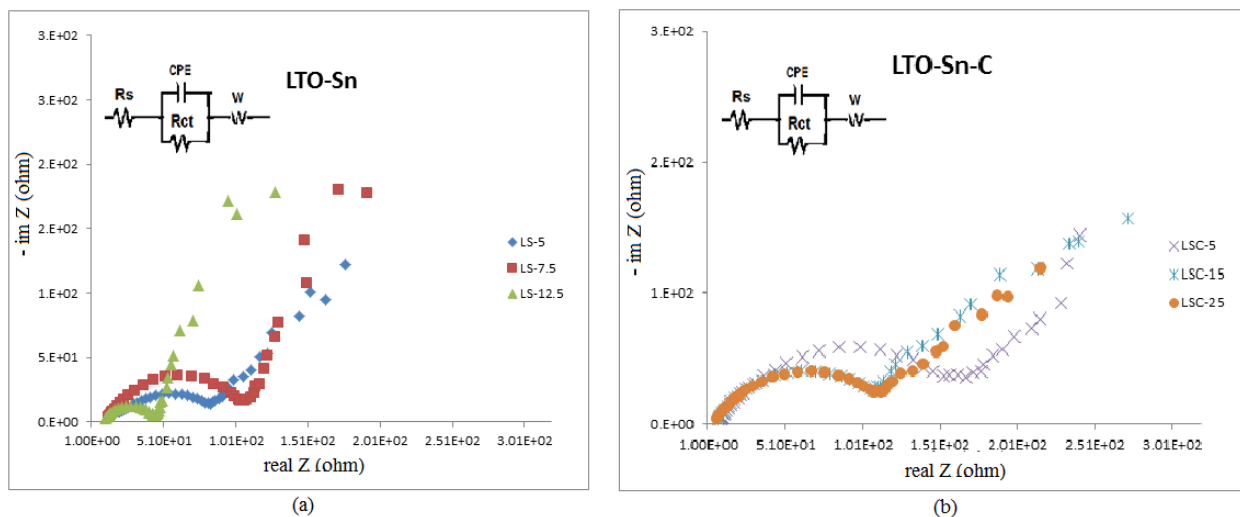

Figure 8 EIS graph spectroscopy of: (a) LTO/Sn; and (b) LTO/Sn@C and the equivalent circuit

From the EIS results, the data was fitted using Z-sim software to obtain Randle's equivalent circuit by selecting the most appropriate circuit model, and run several times until obtaining the fixed value of the component. The estimated equivalent circuit is composed of the electrolyte solution resistance (Rs), which is the intercept impedance on the x-axis, and the electrochemical reaction resistance, or charge transfer resistance (Rct), which is the diameter of the semicircle and double layer capacity of the constant phase element (CPE) in the high-middle frequency range. At low frequencies, the oblique line represents the Li^+ diffusion process, or Warburg

impedance (Fang et al., 2013). The detailed values of Rs, Rct, CPE and Warburg for each sample are listed in Table 5.

Table 5 Parameters of LTO/Sn and LTO/Sn@C anodes from EIS

No.	Anode	Sample	Rs [Ω]	Rct [Ω]	CPE (F)	W (S/s⁵)
1	LTO/Sn	LS-5	18.95	64.42	7.06E-06	0.007200
2	LTO/Sn	LS-7.5	12.84	94.06	5.53E-06	0.003317
3	LTO/Sn	LS-12.5	10.62	34.48	5.85E-06	0.008255
4	LTO/Sn@C	LSC-5	8.95	158.72	7.14E-06	0.005446
5	LTO/Sn@C	LSC-15	7.40	101.06	6.18E-06	0.004297
6	LTO/Sn@C	LSC-25	6.82	105.88	5.55E-06	0.006025

The resistivity value is inversely proportional to that of conductivity. Therefore, the highest conductivity value is in sample LS-12.5. In addition, the Warburg part of the EIS curve from sample LS-12.5 appears to be the steepest curve. Consequently, the diffusion process in this sample is the highest, as seen from the Warburg plot from the EIS curve in Figure 5. Moreover, it is concluded that the addition of carbon increases the Rct value compared to the initial sample LS-7.5 as 0 wt.% carbon. This is shown by a larger semicircle (Rct) value, which is estimated to be mainly attributed to the porous microstructure of carbon, resulting in an increase in bulk resistance (Li et al., 2011).

3.5. Cyclic Voltammetry (CV) Characterization of the LTO Electrodes

A cyclic voltammetry test was conducted to examine the electrochemical performance of the sample; the results are shown in Figure 9. Theoretically, LTO has a peak value of 1.55 V cathodic voltage compared to Li with 175 mAh/g capacity (Sun et al., 2014).

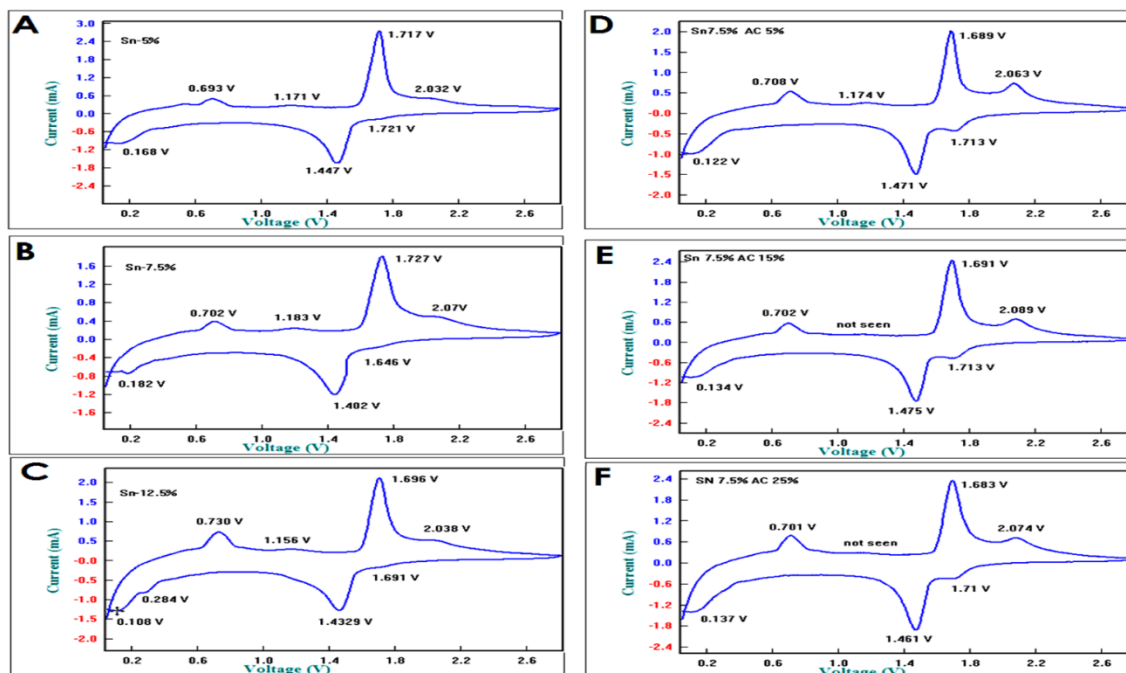Figure 9 CV curve of half-cell, sweep rate 0.1 mVs⁻¹: (a) LS-5; (b) LS-7.5; (c) LS-12.5; (d) LSC-5; (e) LSC-15; (f) LSC-25

As shown by Figures 9a, 9b and 9c, the three cathodic-anodic peaks between 0.1–0.7 V and 1.4–1.8 V are attributed to Sn and LTO anodic peaks respectively. The TiO_2 peak is in the range between 1.6 V and 2.0 V. These peaks are in line with the previous studies, which have shown

that the LTO peaks are at around 1.55 V (Zhao et al., 2015), while the Sn anodic and cathodic peaks are at 0.50 V to 1 V and 0.129 V to 0.752 V (Sivashanmugam et al., 2005) respectively. LTO peak voltages range from 1.4 V to 1.7 V. In the CV curve, the LTO peak appears to dominate, which indicates the significant presence of LTO in the sample. Regarding the Sn peak in each sample, it has different heights because of the Sn concentration. Compared with the LTO peak, the Sn peak tends to be rougher, or not smooth, as the LTO one; this finding is associated with the Sn high volume change during intercalation (Cai et al., 2010). Next, the peak of TiO_2 is in the range between 1.6 V and 2.0 V. The TiO_2 peak is quite small, indicating that the TiO_2 present is not dominant in all the samples.

Furthermore, as shown by Figures 9d, 9e and 9f, the addition of carbon to the LTO/Sn@C sample gives sharper LTO peaks, especially in the cathodic reaction. It can be predicted that in certain porous structures, the intercalation reaction will proceed better. The cathodic and anodic peaks values of all the samples are listed in Table 6.

Table 6 Cathodic and anodic peaks values of the LTO/Sn and LTO/Sn@C anodes

No.	Sample	Sn		LTO		TiO_2	
		Cathodic peak	Anodic peak	Cathodic peak	Anodic peak	Cathodic peak	Anodic peak
1	LS-5	0.168	0.693	1.447	1.717	1.721	2.032
2	LS-7.5	0.182	0.702	1.402	1.727	1.646	2.070
3	LS-12.5	0.284	0.730	1.433	1.696	1.691	2.038
4	LSC-5	0.122	0.708	1.471	1.689	1.713	2.063
5	LSC-15	0.134	0.702	1.475	1.691	1.713	2.089
6	LSC-25	0.137	0.701	1.461	1.683	1.710	2.074

The specific capacity values of all the samples is shown in Table 7.

Table 7 Values of discharge capacities and charge of LTO/Sn and LTO/Sn@C anodes

No.	Anode	Sample	Discharge Capacity (mAh/g)
1	LTO/Sn	LS-5	238.4
2	LTO/Sn	LS-7.5	216.5
3	LTO/Sn	LS-12.5	269.3
4	LTO/Sn@C	LSC-5	270.2
5	LTO/Sn@C	LSC-15	256.9
6	LTO/Sn@C	LSC-25	259.0

In the LTO/Sn sample, the highest value obtained in the sample is that with the composition of 12.5wt% Sn. This is in line with the impedance value results, which decrease proportionally with the Sn content, as shown in Table 5. A lower impedance value means better conductivity, which would lead a higher specific capacity value. Therefore, the addition of Sn succeeded in raising the capacity value of the LTO from its theoretical specific capacity, i.e.: 175 mAh/g, as predicted (Lübke et al., 2015).

In addition, in the LTO/Sn@C, the influence of the addition of carbon increases the specific capacity value of LTO/Sn from 216.5 mAh/g (LS-7.5) to 270.2 mAh/g, 256.9 mAh/g and 259.0 mAh/g in LSC-5, LSC-15 and LSC-25 samples respectively. The highest capacity is achieved with the addition of 5 wt.% carbon. It can be estimated that the porous structure created by the addition of carbon may have a positive influence on the specific capacity value, although the conductivity of the sample decreases because of the addition.

3.6. Charge-Discharge (CD) Characterization of the LTO Electrodes

Charge-discharge testing was conducted to test the battery performance in varying current-rates (C-rates). The C-rate is the unit of speed (charge or discharge) in charging the battery. The CD test was performed on C-rates of 12, 10, 8, 4, 2, 1, 0.5 and 0.2. Battery performance was observed from the capacity achieved at high current (high C-rate), which was 12C in this case. At the rate of 12C, the charge or discharge time will finnish only in 60/12 minutes or 5 minutes. The charge-discharge curve is shown in Figure 10 and the corresponding data is listed in Table 8.
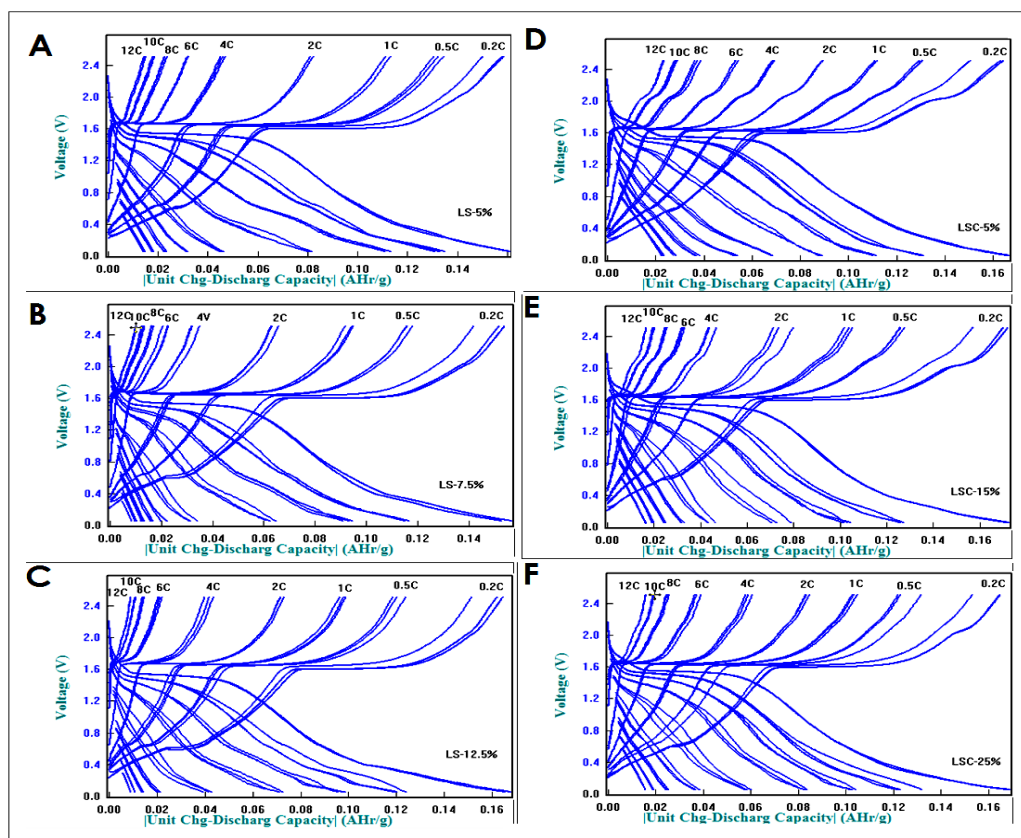

Figure 10 Charge-discharge curves of: (a) LS-5; (b) LS-7.5; (c) LS-12.5; (d) LSC-5; (e) LSC-15; and (f) LSC-25

Table 8 Values of charge and discharge capacity (mAh/g) vs. C-rates

C-rates	LS-5		LS-7.5		LS-12.5		LSC-5		LSC-15		LSC-25	
	+	−	+	−	+	−	+	−	+	−	+	−
0.2	157.7	159.7	153.3	152	164.3	165	163.9	164.3	171.5	171.3	163.8	166.3
0.5	134.2	131.8	11.6	115.8	123.6	122.2	130.5	129.8	127.4	126.1	130.5	131.3
1	112.6	112.5	95.6	92.8	98.7	98.6	111	110.2	105.1	102.1	103.6	103.1
2	82.1	80.1	65.3	64.1	72.9	71.9	88.5	88.2	79.4	78.4	84.3	82.6
4	46.9	45.1	34.6	33.6	41.8	41.3	68.7	67.9	46.8	46.1	60	58.2
6	32.2	31.4	22.5	22.1	21.9	21.6	52.9	52.4	32.1	32.1	38.9	37.7
8	23.7	22.3	17	16.1	14.1	13.6	37.3	36.9	24.7	24.7	25.4	24.3
10	18.6	17.5	12.9	12.8	10.8	10.8	28.7	27.6	19.6	19.4	19.4	19.1
12	14.3	14.1	9.9	9.7	8.9	8.8	22.8	22.6	16.4	16.1	15.9	15.6

Specific capacity at high rates relies greatly on how the mobility of the Li-ions undergo the lithiation-delithiation process. Faster Li-ion mobility leads to a higher overall specific capacity of the material. In addition, the displacement of Li is also affected when the closer the particles

are, the shorter the overall distance travelled. In Table 9, at a current rate of 12C for the LTO/Sn sample, LS-5 achieves the highest capacity, and LS-7.5 the lowest, while for LTO/Sn@C sample, LSC-5 has the highest capacity and LS-12.5 the lowest. Nevertheless, it is worth noting that all the samples could withstand CD testing up to 12C. The plus (+) sign indicates the charge process and the minus (−) sign the discharge process.

All the samples in each C-rate underwent charge-discharge (CD) testing three times. If there is any difference in the value of the capacity obtained in the same C-rates, there is a possibility that the sample is not stable in the redox process. It is interesting to observe all the samples at 0.2C, as seen in Figure 10, which shows that there is a difference in the capacity of the third CD. There was a decline in this CD, showing a decrease in capacity. It is predicted that this is because of the incomplete redox reaction of the sample. If this reaction is not completed, it will form a by-product, which will obstruct the flow of electrons. The by-product is usually deposited on the surface area of the anode, which leads to decrease in the redox reaction.

4.   CONCLUSION

The compounds LTO/Sn and LTO/Sn@C were successfully synthesized using sol-gel, the addition of activated carbon and a solid state process, while also obtaining a reasonably high surface area and minimum aggregation. There is no single phase in any of the samples resulting from more than one peak on the CV curve present. The role of the addition of Sn to LTO to form LTO/Sn succeeded in raising the capacity value of the LTO from its theoretical specific capacity of 175 mAh/g. On the other hand, in the LTO/Sn@C the influence of the addition of carbon increases the specific capacity value compared to LTO/Sn. However, the main obstacle to obtaining consistent results in this research may have been the impurities in the carbon contained in the sample, such as the presence of ash, which inhibits the flow of electrons. The CV curve shows that all the samples have more than one peak. This is consistent with the XRD results, where there are phases of TiO_2, Sn and LTO in the sample. The addition of Sn and carbon generally succeeded in raising capacity. At a high C-rate, the addition of carbon raises the specific capacity value. LTO with a composition of 7.5 wt.% Sn and 5 w.t% carbon (LSC-5) creates the optimum conditions to achieve a specific capacity of 270.2 mAh/g, which is much higher than the theoretical capacity of LTO of 175 mAh/g.

5.   ACKNOWLEDGEMENT

6.   REFERENCES

Abdurrahman, N.M., Priyono, B., Syahrial, A.Z., Subhan, A., 2017. Effect of Acetylene Black Content in $Li_4Ti_5O_{12}$ Xerogel Solid-state Anode Materials on Half-cell Li-ion Batteries Performance. *Journal of Physics: Conference Series*, Volume 877, 012008.

Ariyoshi, K., Yamato, R., Ohzuku, T., 2005. Zero-strain Insertion Mechanism of Li[Li1/3Ti 5/3]O4 For Advanced Lithium-ion (Shuttlecock) Batteries. *Electrochimica Acta*, Volume 51(6), pp. 1125–1129

Aurbach, D., Nimberger, A., Markovsky, B., Levi, E., Sominski, E., Gedanken, A., 2002. Nanoparticles of SnO Produced by Sonochemistry as Anode Materials for Rechargeable Lithium Batteries. *Chemistry of Material*, Volume 14(7), pp. 4155–4163

Bayati, B., Babaluo, A.A., Karimi, R., 2008. Hydrothermal Synthesis of Nanostructure NaA Zeolite: The Effect of Synthesis Parameters on Zeolite Seed Size and Crystallinity. *Journal*

of the European Ceramic Society, Volume 28(14), pp. 2653–2657

Cai, R., Yu, X., Liu, X., Shao, Z., 2010. Li₄Ti₅O₁₂/Sn Composite Anodes for Lithium-ion Batteries: Synthesis and Electrochemical Performance. *Journal of Power Sources*, Volume 195(24), pp. 8244–8250

Chen, M., Bae, J., 2006. Preparation of Carbon-Coated TiO₂ at Different Heat Treatment Temperatures and Their Photoactivity. *Carbon Science*, Volume 7(4), pp. 259–265

Crosnier, O., Brousse, T., Devaux, X., Fragnaud, P., Schleich, D.M., 2001. New Anode Systems for Lithium Ion Cells. *Journal of Power Sources*, Volume 94(2), pp. 169–174

Egashira, M., Takatsuji, H., Okada, S., Yamaki, J.I., 2002. Properties of Containing Sn Nanoparticles Activated Carbon Fiber for a Negative Electrode in Lithium Batteries. *Journal of Power Sources*, Volume 107(1), pp. 56–60

Fang, W., Zuo, P., Ma, Y., Cheng, X., Liao, L., Yin, G., 2013. Facile Preparation of Li₄Ti₅O₁₂/AB/MWCNTs Composite with High-rate Performance for Lithium Ion Battery. *Electrochimica Acta*, Volume 94, pp. 294–299

Kim, Y., Yoon, Y., Shin, D., 2009. Fabrication of Sn/SnO₂ Composite Powder for Anode of Lithium Ion Battery by Aerosol Flame Deposition. *Journal of Analytical and Applied Pyrolysis*, Volume 85(1–2), pp. 557–560

Li, B., Ning, F., He, Y., Du, H., Yang, Q., Kang, F., Hsu, C., 2011. Synthesis and Characterization of Long Life Li₄Ti₅O₁₂/C Composite using Amorphous TiO₂ Nanoparticles. *International Journal of Electrochemical Science*, Volume 6, pp. 3210–3223

Li, H., Shen, L., Zhang, X., Wang, J., Nie, P., Che, Q., Ding, B., 2013. Nitrogen-doped Carbon Coated Li₄Ti₅O₁₂ Nanocomposite: Superior Anode Materials for Rechargeable Lithium Ion Batteries. *Journal of Power Sources*, Volume 221, pp. 122–127

Liang, S., Zhu, X., Lian, P., Yang, W., Wang, H., 2011. Superior Cycle Performance of Sn@C/graphene Nanocomposite as an Anode Material for Lithium-ion Batteries. *Journal of Solid State Chemistry*, Volume 184(6), pp. 1400–1404

Lübke, M., Johnson, I., Makwana, N.M., Brett, D., Shearing, P., Liu, Z., Darr, J.A., 2015. High Power TiO₂ and High Capacity Sn-doped TiO₂ Nanomaterial Anodes for Lithium-ion Batteries. *Journal of Power Sources*, Volume 294, pp. 94–102

Priyono, B., Syahrial, A.Z., Yuwono, A.H., Kartini, E., Marfelly, M., Rahmatulloh, W.M.F., 2015. Synthesis of Lithium Titanate (Li₄Ti₅O₁₂) through Hydrothermal Process by using Lithium Hydroxide (LiOH) and Titanium Dioxide (TiO₂) Xerogel. *International Journal of Technology*, Volume 6(4), pp. 555–564

Sivashanmugam, A., Kumar, T.P., Renganathan, N.G., Gopukumar, S., Wohlfahrt-Mehrens, M., Garche, J., 2005. Electrochemical Behavior of Sn/SnO₂ Mixtures for Use as Anode in Lithium Rechargeable Batteries. *Journal of Power Sources*, Volume 144(1), pp. 197–203

Sofyan, N., Putro, D.Y., and Zulfia, A., 2016. Performance of Vanadium-doped LiFePO₄/C Used as a Cathode for a Lithium Ion Battery. *International Journal of Technology*, Volume 7(8), pp. 1225–1235

Sun, X., Hegde, M., Zhang, Y., He, M., Gu, L., Wang, Y., Shu, J., Radovanovic, P.V., Cui, B., 2014. Structure and Electrochemical Properties of Spinel Li₄Ti₅O₁₂ Nanocomposites as Anode for Lithium-ion Battery. *International Journal of Electrochemical Science*, Volume 9(4), pp. 1583–1596

Syahrial, A.Z., Aldy, F., Priyono, B., Subhan, A., 2018a. Enhanced Electrochemical Performances of Li₄Ti₅O₁₂/Sn Composites Anode via Sol-hydrothermal Method for Lithium Ion Batteries. *IOP Conference Series: Earth and Environmental Science*, Volume 105

Syahrial, A.Z., Margaretha, Y.R., Priyono, B., Subhan, A., 2018b. Synthesis of LTO Nanorods with AC/Nano-Si Composites as Anode Materials for Lithium-ion Batteries. *International Journal of Technology*, Volume 9(6), pp. 1225–1235

Yi, T.-F., Yang, S.-Y., Tao, M., Xie, Y., Zhu, Y.-R., Zhu, R.-S., 2014. Synthesis and Application

of a Novel Li$_4$Ti$_5$O$_{12}$ Composite as Anode Material with Enhanced Fast Charge-discharge Performance for Lithium-ion Battery. *Electrochimica Acta*, Volume 134, pp. 377–383

Zhao, B., Ran, R., Liu, M., Shao, Z., 2015. A Comprehensive Review of Li$_4$Ti$_5$O$_{12}$-based Electrodes for Lithium-ion Batteries: The Latest Advancements and Future Perspectives. *Materials Science & Engineering: Reports*, Volume 98, pp. 1–71